Synchronization of the Carrier Wave of Parallel Three-Phase Inverters With Virtual Oscillator Control

Jian Hu, *Student Member, IEEE*, and Hao Ma, *Member, IEEE*

***Abstract*—In this paper, a method to synchronize the carrier wave of parallel three-phase inverters without communication is proposed. This method is based on the digital-based virtual dead-zone oscillators coupled with each other through electrical connections between parallel inverters. These oscillators are synchronized based on the phenomenon of synchronization in networks of coupled oscillators. Thus, the carrier waves of different inverters are confirmed to be synchronized since they are generated by the oscillators. The model of the circulating current and the sufficient condition of global synchronization of oscillators are derived in this paper. The methodology for controller design is outlined based on the aforementioned analysis. Experimental results for a system with three inverters are given to illustrate the effectiveness of the proposed control.**

***Index Terms*—Circulating currents, dead-zone oscillators, modulation, nonlinear control, voltage source inverters (VSIs).**

I. Introduction

THE parallel operation of voltage source inverters has become a popular choice in high power applications due to its many advantages, such as larger system capacity, increased system robustness, easy and flexible implementation, and lower cost for repair and replacement of each failure [1]–[5]. In a parallel connection of voltage-source inverters, one of the major concerns is the circulating currents between inverters, since it reduces the power rating and efficiency of the system [6], [7]. The circulating current can be generated by the loose of the synchronization between inverters, mismatched output inductance, measuring errors, and discretization of the controllers [8], [9]. In order to suppress circulating currents, various control techniques have been introduced including voltage frequency droop control [10], circular chain-control [11], and harmonic-elimination pulse-width modulation (PWM) [12]. By introducing these techniques, most of the fundamental and low-order harmonic circulating currents can be eliminated.

The nonsynchronous carrier waves between different inverter are another important cause of the circulating current. It is found that the amplitude of switching circulating current is inversely proportional to the switching frequency [13]. Hence, it will be come an important part of circulating current when low switching frequency is required to reduce the switching loss. However, the aforementioned techniques lack ability to suppress such current since they only deal with reference modulation waves. One solution to suppress such circulating current is to introduce an isolating transformer or mutual inductance at ac side of each inverter [14], but it will make the inverter costly and bulky. Another solution which can eliminate such circulating current is to acquire ideal operation status of the parallel inverter system which requires uniform modulation of every inverter [15]. This status can be achieved via a central controller which controls all inverters [16] or communication between inverters to synchronize the carrier wave [17]. But these methods increase the complexity of the controller, impose restrictions on the locations of the inverter and degrade the reliability of system.

Recently, a virtual oscillator control (VOC) which can synchronize nonlinear electrical circuit without communication was proposed in [18]. Such control has been used to synchronize reference modulation wave of parallel connected inverter to share the load in proportion to their ratings and eliminated the fundamental circulating currents [19]. Compared to droop control and its variants, this control achieves minimal deviations of the system frequency with variations in load and simplifies the controller as it requires neither filter nor power calculation [20]. However, this method only deal with the reference modulation wave and cannot eliminate the switching frequency circulating currents.

Inspired by the aforementioned control strategies, a VOC-based synchronization method for the carrier waves is proposed in this paper. The method uses virtual oscillator to generate the carrier wave and synchronizes them with the electrical coupling between paralleled inverters. Based on the characteristic of the phenomenon of synchronization in the networks of coupled oscillators, this method is able to synchronize carrier wave among different inverters without communication and independent to the load and the number of the inverters in the system.

The remainder of this paper is organized as follows. In Section II, the analysis of the switching circulating current in a parallel inverter system is carried out. In Section III, the coordinate system where the control strategy is implemented is first selected, then the detailed control implementation of the proposed control is given. Finally, the equations that describe the coupling of the virtual oscillators, sufficient conditions for the global asymptotic synchronization are outlined. The methodology for parameters selection is given in Section IV,

Manuscript received July 22, 2015; revised October 16, 2015; accepted March 10, 2016. Date of publication March 22, 2016; date of current version May 9, 2017. This work was supported by National Natural Science Foundation of China (51177149), and Specialized Research Fund for the Doctoral Program of Higher Education (20130101110108). Recommended for publication by Associate Editor J. R. Espinoza.

The authors are with the College of Electrical Engineering, Zhejiang University, Hangzhou 310027, China (e-mail: hujian_0009991@163.com; mahao@zju.edu.cn.).

Color versions of one or more of the figures in this paper are available online at http://ieeexplore.ieee.org.

Digital Object Identifier 10.1109/TPEL.2016.2544944

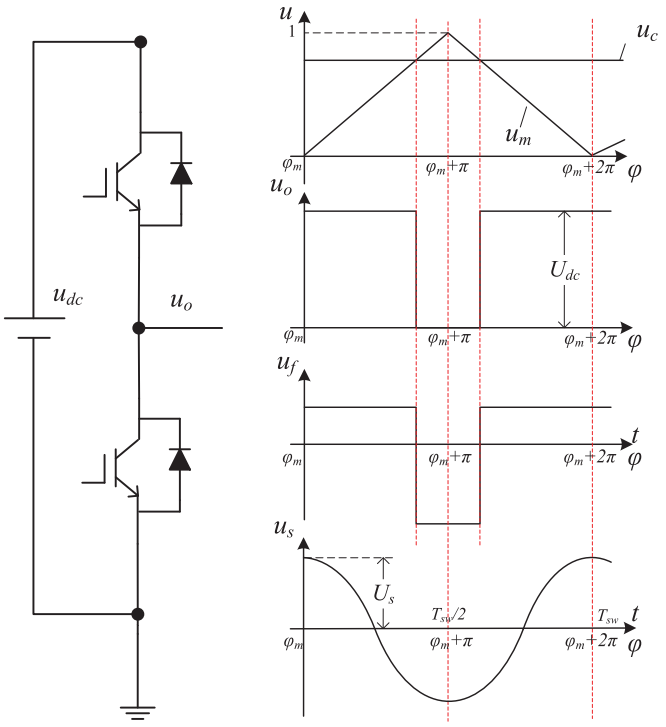

Fig. 1. Waveforms in this figure are organized as follows (from top to bottom): (a) Carrier wave u_m and reference modulation wave u_c. (b) The output voltage of bridge u_o. (c) The output voltage without dc component u_f. (d) The switching frequency components of output voltage u_s.

followed by the experimental results of steady state and dynamic in Section V. Finally, a conclusion is highlighted in Section VI.

II. Mathematic Model of Switching Circulating Current

In this section, the mathematic model of the switching circulating current among paralleled inverters is given and detailed discussions are given. First, the relationship between carrier wave and the switching frequency components of the output voltage of inverter is discussed. Based on this discussion, the model of the switching circulating current of the system is derived.

A. Relationship Between Carrier Wave and Switching Frequency Components of the Output Voltage

The output voltage of each inverter leg u_o is determined by two waves: carrier wave u_m and reference modulation wave u_c as shown in Fig. 1. The duty ratios are determined by u_c and the switching times are determined by u_m. The output voltage of the bridge can be expressed as

$$u_o = \begin{cases} 0 & \left|t - \dfrac{T_{\rm sw}}{2}\right| < \dfrac{\tau}{2} \\ U_{\rm dc} & \dfrac{\tau}{2} < \left|t - \dfrac{T_{\rm sw}}{2}\right| < \dfrac{T_{\rm sw}}{2} \end{cases} \tag{1}$$

where $T_{\rm sw}$, τ represent the switching period and pulse width, respectively. The Fourier series expansion of the output voltage u_o is

$$u_o = U_{\rm dc}\left[\frac{\tau}{T_{\rm sw}} + \sum_{n=1}^{\infty}\frac{2}{n\pi}\sin\left(\frac{\pi n\tau}{T_{\rm sw}}\right)\cos\left(\frac{2\pi n}{T_{\rm sw}}t\right)\right]. \tag{2}$$

It is easy to derive from the principals of PWM that

$$d = \frac{\tau}{T_{\rm sw}} = u_c \tag{3}$$

where d represent the duty ratio of the PWM waves. Combining (2) and (3) yields

$$u_o = U_{\rm dc}\left[d + \sum_{n=1}^{\infty}\frac{2}{n\pi}\sin(\pi n d)\cos\left(\frac{2\pi n t}{T_{\rm sw}}\right)\right]. \tag{4}$$

The dc components of the u_o is related to the reference modulation wave u_c, which changes at fundamental frequency. Hence, it can be ignored while discussing switching frequency components. The high frequency components can also be ignored since their amplitude is relatively small compared to the switching frequency components.

In order to link the time domain and frequency domain, the phase angle of the start time of the carrier wave is defined as φ_m, and the palstance of the switching frequency system ω_s is defined as

$$\omega_s \triangleq \frac{2\pi}{T_{\rm sw}}. \tag{5}$$

The switching frequency component u_s can be expressed as

$$u_s = \frac{2U_{\rm dc}}{\pi}\sin(\pi d)\sin\left(\omega_s t + \varphi_m + \frac{\pi}{2}\right). \tag{6}$$

Thus, voltage phasor of switching frequency component is

$$\dot{U}_s = \frac{2U_{\rm dc}}{\pi}\sin(\pi d)\angle(\varphi_m + \frac{\pi}{2}). \tag{7}$$

From (7), two conclusions can be drawn:

1) The amplitude of the switching frequency phasor of the output voltage is determined by the duty ratio d. The amplitude reaches it maximum when d is 0.5. The component can be eliminated when d is 1 or 0.
2) The phase of the switching frequency phasor is 90° ahead of the phase of carrier wave.

B. Circulating Current Between Paralleled Inverters

Based on (7), the voltage phasor of switching components of three phases can be expressed as

$$\begin{cases} \dot{U}_{\rm sa} = \dfrac{2U_{\rm dc}}{\pi}\sin(\pi d_a)\angle(\varphi_m + \dfrac{\pi}{2}) \\ \dot{U}_{\rm sb} = \dfrac{2U_{\rm dc}}{\pi}\sin(\pi d_b)\angle(\varphi_m + \dfrac{\pi}{2}) \\ \dot{U}_{\rm sc} = \dfrac{2U_{\rm dc}}{\pi}\sin(\pi d_b)\angle(\varphi_m + \dfrac{\pi}{2}) \end{cases}. \tag{8}$$

Since the three bridges of the inverter often share common carrier wave, the phases of three-bridge output voltage are the same. However, the magnitudes of them are nonidentical since the reference modulation waves which determine the magnitude are different between three phases. Obviously the source of three phases is imbalanced. The phasor diagram of the system

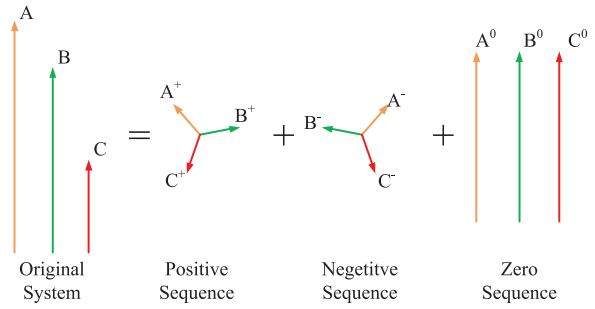

Fig. 2. Phasor diagrams of asymmetric voltage and the positive, negative, and zero sequence system.

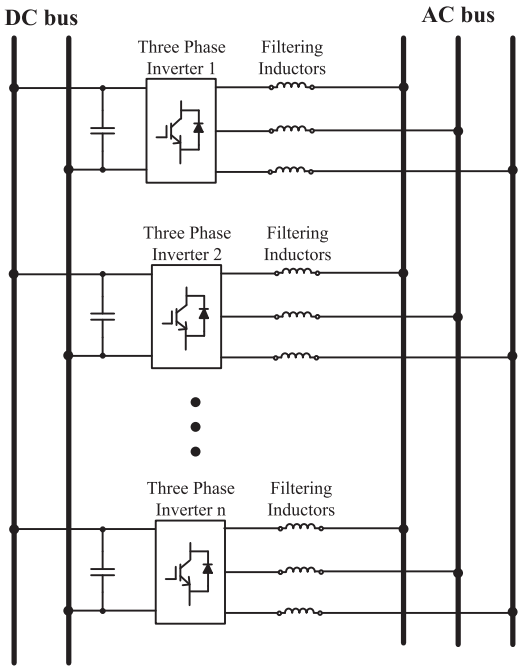

Fig. 3. Parallel inverter system without isolation.

can be expressed as Fig. 2. This asymmetric characteristic of the voltage source of the circuit makes it complex to analyze the circuiting current. In order to simplify the analysis, method of symmetrical components is used to decompose the system into three symmetrical systems: positive, negative, and zero sequence systems. The decomposition is realized by

$$\begin{bmatrix} \dot{U}^{+} \\ \dot{U}^{-} \\ \dot{U}^{0} \end{bmatrix} = \frac{1}{3} \begin{bmatrix} 1 & e^{j\frac{2\pi}{3}} & e^{j\frac{4\pi}{3}} \\ 1 & e^{j\frac{4\pi}{3}} & e^{j\frac{2\pi}{3}} \\ 1 & 1 & 1 \end{bmatrix} \begin{bmatrix} \dot{U}_a \\ \dot{U}_b \\ \dot{U}_c \end{bmatrix} \tag{9}$$

where $\dot{U^{+}}$, $\dot{U^{-}}$, and $\dot{U^{0}}$ represent the phasors positive, negative, and zero sequence voltages, respectively.

Based on this method, the phasor diagram of the asymmetric voltage source and the results of the division are depicted in Fig. 2.

The parallel inverter system depicted in Fig. 3 can be divided into three symmetric systems.

The equivalent circuit of the three systems is shown in Fig. 4, where $\dot{U}_x^{+}$, $\dot{U}_x^{-}$, and $\dot{U}_x^{0}$ represent the positive, negative, and zero sequence voltage phasors of each inverter, respectively, $\dot{U}_l^{+}$, $\dot{U}_l^{+}$, and $\dot{U}_l^{+}$ stand for the positive, negative, and zero sequence voltage phasors of load, $\dot{I}_x^{+}$, $\dot{I}_x^{-}$, and $\dot{I}_x^{0}$ are on behalf of the positive, negative, and zero sequence current phasors of each inverter, respectively; Z^{+}, Z^{-}, Z^{0} represent the positive, negative, and zero sequence of load impedances, respectively, Z_o stand for the impedance of the output filter of each inverter.

According to node analysis, the load voltage of the system can be expressed as follows:

$$\begin{cases} \dot{U}_l^{+} = \sum_{j=1}^{n} \dfrac{\dot{U}_j^{+}}{Z_o} \Big/ \left(\dfrac{N}{Z_o} + \dfrac{1}{Z^{+}} \right) \\ \dot{U}_l^{-} = \sum_{j=1}^{n} \dfrac{\dot{U}_j^{-}}{Z_o} \Big/ \left(\dfrac{N}{Z_o} + \dfrac{1}{Z^{-}} \right) \\ \dot{U}_l^{0} = \sum_{j=1}^{n} \dfrac{\dot{U}_j^{0}}{Z_o} \Big/ \left(\dfrac{N}{Z_o} + \dfrac{1}{Z^{0}} \right). \end{cases} \tag{10}$$

The current phasors of each inverter can be expressed as

$$\begin{cases} \dot{I}_x^{+} = (\dot{U}_x^{+} - \dot{U}_l^{+})/Z_o \\ \dot{I}_x^{-} = (\dot{U}_x^{-} - \dot{U}_l^{-})/Z_o \\ \dot{I}_x^{0} = (\dot{U}_x^{0} - \dot{U}_l^{0})/Z_o \end{cases} \qquad x \in \{1, 2 \ldots n\}. \tag{11}$$

The circulating current of each inverter is defined in below [21]

$$C_x \triangleq \sum_{j=1}^{n} \frac{i_x - i_j}{N} \qquad x \in \{1, 2 \ldots n\}. \tag{12}$$

Combining (11) and (12), the phasors of the circulating current of each inverter can be expressed as

$$\begin{aligned} \dot{C}_x^{+} &= \frac{\dot{U}_x^{+} - \frac{1}{N}\sum_{j=1}^{N} \dot{U}_j^{+}}{Z_o} \\ \dot{C}_x^{-} &= \frac{\dot{U}_x^{-} - \frac{1}{N}\sum_{j=1}^{N} \dot{U}_j^{-}}{Z_o} \qquad x \in \{1, 2 \ldots n\} \\ \dot{C}_x^{0} &= \frac{\dot{U}_x^{0} - \frac{1}{N}\sum_{j=1}^{N} \dot{U}_j^{0}}{Z_o} \end{aligned} \tag{13}$$

where $\dot{C}_x^{+}$, $\dot{C}_x^{+}$, and $\dot{C}_x^{0}$ represent the positive, negative, and zero sequence circulating current phasors of each inverter, respectively.

Therefore, the switching circulating current of each inverter can be expressed as

$$C_x = C_x^{0} + C_x^{+} + C_x^{-} \qquad x \in \{1, 2 \ldots n\}. \tag{14}$$

Obviously, switching circulating current C_x would be eliminated, if all the switching frequency components of different inverters are the same. Hence, it is essential to synchronize carrier wave among parallel inverters to eliminate the switching circulating current.

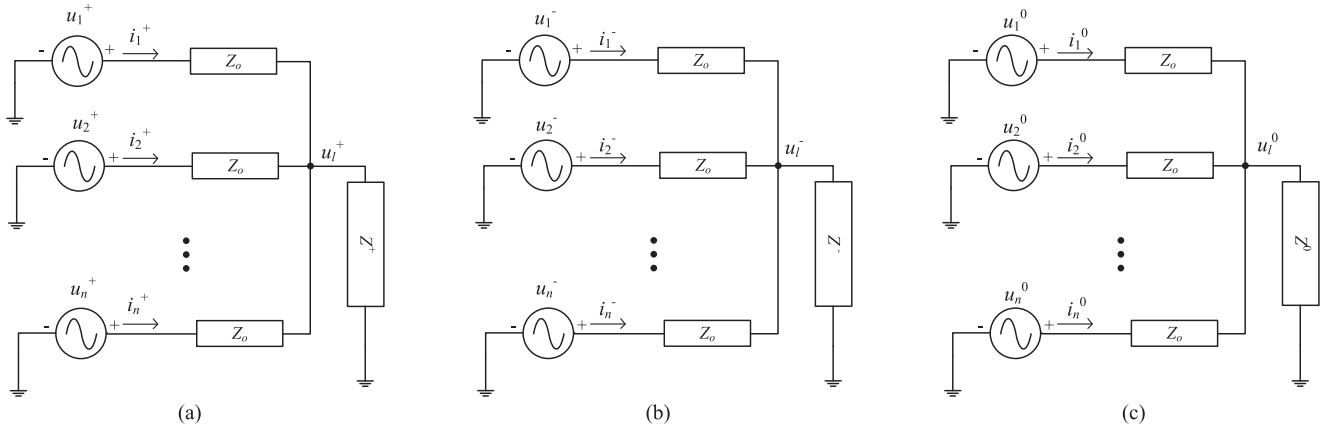

Fig. 4. Equivalent model of switching circulating current of phase A of parallel inverter system. (a) Positive sequence system. (b) Negative sequence system. (c) Zero sequence system.

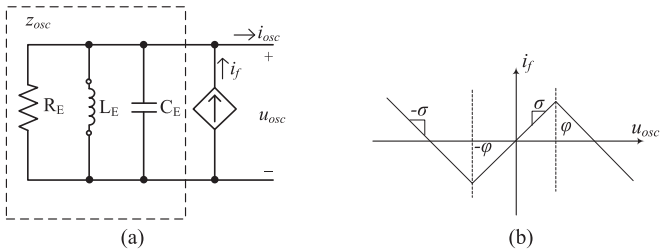

Fig. 5. Structure of the dead-zone oscillator. (a) Electrical circuit. (b) Characteristics of voltage independent current source.

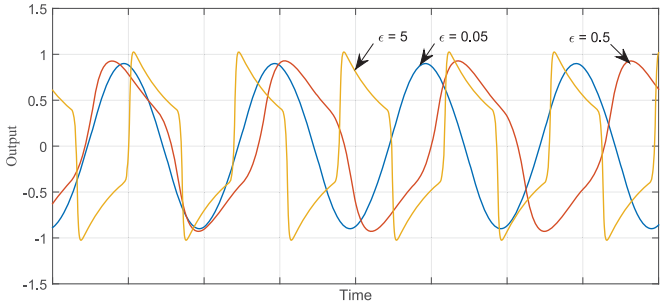

Fig. 6. Output of virtual dead-zone oscillator with different ϵ.

III. Control System Description

In this section, the basic principles of virtual oscillator which serve as the core of the controller are first reviewed. Then, the structure of proposed controller is introduced. In the end, equations that describe the couplings of the virtual oscillator of different inverters and a sufficient condition for synchronization of them are outlined.

A. Nonlinear Dead-Zone Oscillator

Before introducing the synchronization of the carrier with virtual oscillator, the basic principles of virtual oscillator is reviewed.

The electrical schematic of the nonlinear dead-zone oscillator is shown in Fig. 5. The linear subsystem is a passive RLC circuit which determines the oscillator frequency

$$f_{\rm osc} = \frac{1}{2\pi\sqrt{L_E C_E}}. \tag{15}$$

The voltage-independent current source is the energy source of the oscillator, the output of which is defined as

$$f(u_{\rm osc}) = \begin{cases} -2\sigma\varphi - \sigma u_{\rm osc} & u_{\rm osc} < \varphi \\ \sigma u_{\rm osc} & -\varphi < u_{\rm osc} < \varphi \\ 2\sigma\varphi - \sigma u_{\rm osc} & u_{\rm osc} > \varphi \end{cases}. \tag{16}$$

The electric equation of the oscillator can be described as

$$u_{\rm osc} = Z_{\rm osc}(i_f - i_{\rm osc}) \tag{17}$$

where $Z_{\rm osc}$ is the impedance of passive RLC circuit

$$Z_{\rm osc}(s) = R||sL||(sC)^{-1} = \frac{RLs}{RLCs^2 + Ls + R}. \tag{18}$$

Another important parameter for the oscillator can be defined as

$$\epsilon = \sqrt{\frac{L_E}{C_E}}\left(\sigma - \frac{1}{R_E}\right). \tag{19}$$

With small value of ϵ, the output of the oscillator approximates an ideal sinusoid in the time domain as shown in Fig. 6.

B. Proposed Control Structure

In order to use virtual oscillators to synchronize the carrier waves of paralleled inverters, two requirements should be met: 1) the virtual oscillators should be coupled through electrical link between inverters; and 2) the carrier wave should be generated with the output of virtual oscillator so that the synchronization of carrier wave can be guaranteed if the virtual oscillators are synchronized. To fulfill the aforementioned requirements, the control structure of the VOC-based carrier synchronization of one inverter in the system is depicted in Fig. 7(a).

The currents of the three phase are added to get the zero sequence current i_0, which then passes through a bandpass filter to eliminate the current other than switching frequency. After the normalization with constant k_i, the current is sent to the

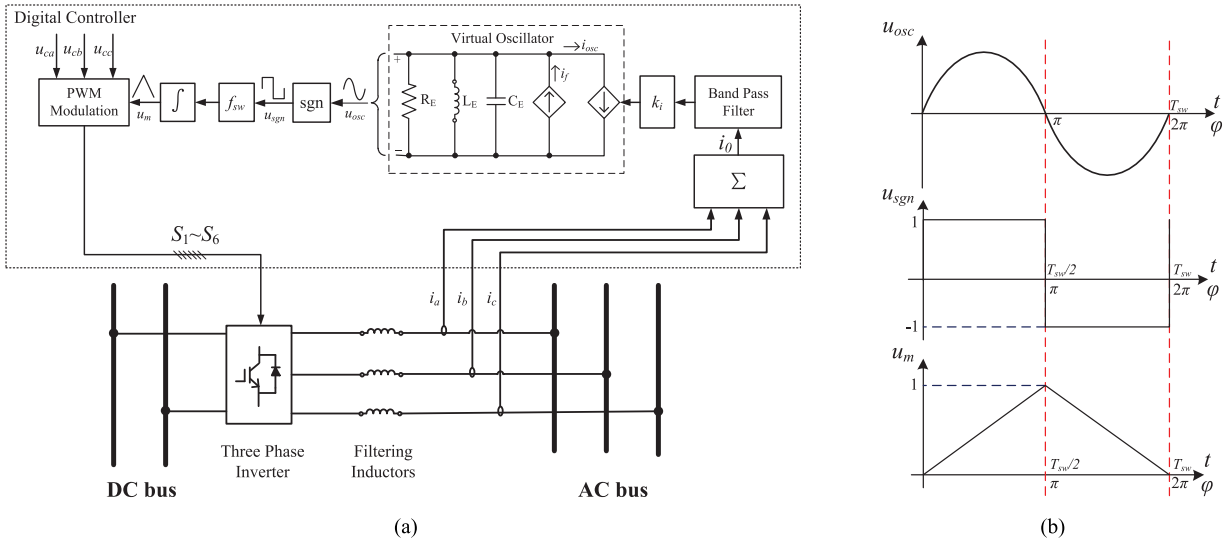

Fig. 7. (a) Control structure of VOC-based carrier synchronization. (b) Waveforms of $u_{\rm osc}$, $u_{\rm sgn}$, and u_m .

virtual oscillator serving as the output current $i_{\rm osc}$. With zero sequence currents as the input, the virtual oscillators are coupled with each other through zero sequence system discussed in Section II.

The output voltage of the oscillator $u_{\rm osc}$ is used to generate the carrier wave of the inverter according to following steps. First, the output voltage $u_{\rm osc}$ is reshaped by signum function to a square wave $u_{\rm sgn}$. This wave then passes through an integrator to generate a triangle wave u_m . The waveforms of $u_{\rm osc}$, $u_{\rm sgn}$, and u_m is depicted in Fig. 7(b). u_m serves as the carrier wave with modulate reference modulation waves to generate the PWM signals $S_1 \sim S_6$ to control the three-phase inverter.

C. Network Analysis and Sufficient Condition of Synchronization of Virtual Oscillator

The goal of the proposed control is to synchronize the carrier waves of different inverters. This can be achieved by the synchronization of the virtual oscillators of different inverters, since the phase and frequency of the carrier wave is determined by the output voltage of the virtual oscillator as shown in Fig. 7(b). Thus, the goal of the controller is equivalent to the synchronization of the output voltage $u_{\rm osc}$ of each inverter with electrical coupling among them. In order to derive the sufficient condition of synchronization of virtual oscillator for different inverters, the model of the electrical coupling among them is first established.

Combining (7) and (9), the phasor of zero sequence voltage of xth inverter can be expressed as follows:

$$\dot{U}_x^0 = \frac{2U_{\rm dc}}{3\pi}[\sin(\pi d_{\rm ax}) + \sin(\pi d_{\rm bx}) + \sin(\pi d_{\rm cx})]\angle(\varphi_m + \frac{\pi}{2}). \tag{20}$$

From Fig. 7(b), it can be concluded that the output of oscillator $u_{\rm osc}$ and the carrier wave u_m have the same phase. Based on the discussion above, the relationship between the phasor of the output voltage $\dot{U}_{{\rm osc}x}$ and that of zero sequence voltage $\dot{U}_x^0$ can expressed by

$$\dot{U}_x^0 = A_{0x}\angle(\varphi_{\rm osc} + \frac{\pi}{2}) = \frac{A_{0x}}{A_{{\rm osc}x}}\angle\frac{\pi}{2} * \dot{U}_{{\rm osc}x} \tag{21}$$

where $A_{{\rm osc}x}$, $\varphi_{\rm osc}$ stand for the amplitude and phase of the oscillator output voltage $u_{{\rm osc}x}$, respectively, and A_{0x} represents amplitude of $\dot{U}_x^0$ which is determined by the duty ratios and dc-link voltage

$$A_{0x} = \frac{2U_{\rm dc}}{3\pi}\sin(\pi d_{\rm ax}) + \sin(\pi d_{\rm bx}) + \sin(\pi d_{\rm cx}). \tag{22}$$

Convert (21) into s-domain[1]

$$u_x^0(s) = G_{\rm ux}(s)u_{{\rm osc}x}(s) \tag{23}$$

where

$$G_{\rm ux}(s) = \frac{A_{0x}}{A_{{\rm osc}x}}e^{j\frac{\pi}{2}}. \tag{24}$$

The relationship between the output currents of the inverter and oscillator can be expressed as

$$i_{{\rm osc}x} = k_i G_{\rm fx}(s)i^0(s) = G_{\rm ix}(s)i^0(s) \tag{25}$$

where $G_{\rm fx}(s)$ is the transfer function of the bandpass filter of xth inverter. The model of electrical coupling between virtual oscillators can be depicted in Fig. 8.

Based on (11), the zero-sequence output current of each inverter i_x^0 is

$$i_x^0(s) = Z_o(s)^{-1}(u_x^0(s) - u_l^0(s)). \tag{26}$$

Substituting the voltage and current from (23) into (26), the output current $i_{{\rm osc}x}$ and voltage $u_{{\rm osc}x}$ of each oscillator are related by

$$i_{{\rm osc}x} = {Z_o}^{-1}(s)(G_{\rm ix}(s)G_{\rm ux}(s)u_{{\rm osc}x}(s) - G_{\rm ix}(s)u_l^0(s)). \tag{27}$$

[1] 90° phase lead is equivalent to $e^{j\frac{\pi}{2}}$.

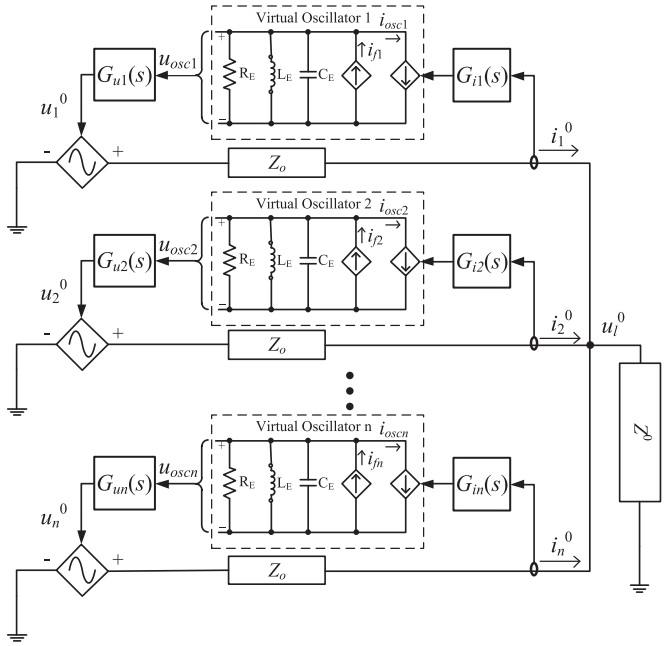

Fig. 8. Model of electrical coupling between oscillators of different inverters.

Solving for $u_{\mathrm{osc}x}$, the following can be obtained:

$$u_{\mathrm{osc}x} = (G_{\mathrm{ix}}(s)G_{\mathrm{ux}}(s))^{-1}(Z_o(s)i_{\mathrm{osc}x}(s) + G_{\mathrm{ix}}(s)u_l^0(s)). \tag{28}$$

The zero-sequence load voltage can be expressed as

$$u_l^0 = Z^0(s)\sum_{x=1}^{N} i_x^0(s) = Z^0(s)\sum_{x=1}^{N}(G_{\mathrm{ix}}(s)i_{\mathrm{osc}x}(s)). \tag{29}$$

Substituting (29) and into (28) yields

$$u_{\mathrm{osc}x} = \frac{Z_o(s)i_{\mathrm{osc}x}(s) + Z^0(s)\sum_{k=1}^{N}(G_{\mathrm{ik}}(s)i_{\mathrm{osc}k}(s))}{G_{\mathrm{ix}}(s)G_{\mathrm{ux}}(s)}. \tag{30}$$

Assuming the reference modulation waves of each inverter are synchronized,[2] the duty ratios of PWM signals of the each inverter are nearly identical. Based on (22), one can conclude that the A_{0x} is identical among different inverters. $A_{\mathrm{osc}x}$ is the same among different inverters if the parameters of the oscillator of each inverter are same. Therefore, the G_{ux} is the same between different inverters. Similarly, $G_{\mathrm{ix}}(s)$ can also considered to be identical if the parameters of bandpass filter and current gains of each inverter are same.

Thus, the matrix form of (30) collecting all voltages and currents of different oscillators is

$$u_{\mathrm{osc}}(s) = \frac{[Z_o(s)I + Z^0(s)A]i_{\mathrm{osc}}(s)}{G_i(s)G_u(s)} \tag{31}$$

where the vectors of the output voltages and currents are denoted by $u_{\mathrm{osc}} = [u_{\mathrm{osc}1}, \ldots, u_{\mathrm{osc}n}]^T$ and $i_{\mathrm{osc}} = [i_{\mathrm{osc}1}, \ldots, i_{\mathrm{osc}n}]^T$.

[2]If the reference modulation waves of different inverters are out of synchronization, large amplitude of fundamental frequency circulating current will occur. Hence, it is meaningless to discuss the synchronization of carrier wave under such condition.

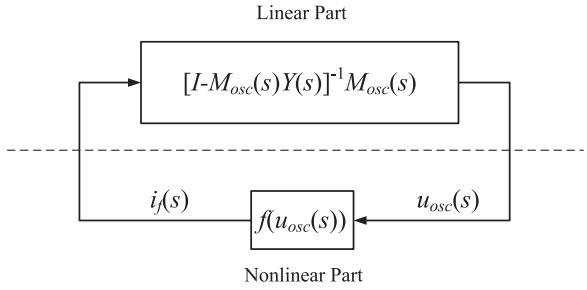

Fig. 9. Block diagram compartmentalizing linear part and nonlinear part of system.

And I and A are N order matrix defined as

$$I \triangleq \begin{bmatrix} 1 & 0 & \cdots & 0 \\ 0 & 1 & \cdots & 0 \\ \vdots & \vdots & \ddots & \vdots \\ 0 & 0 & \cdots & 1 \end{bmatrix}, \quad A \triangleq \begin{bmatrix} 1 & 1 & \cdots & 1 \\ 1 & 1 & \cdots & 1 \\ \vdots & \vdots & \ddots & \vdots \\ 1 & 1 & \cdots & 1 \end{bmatrix}. \tag{32}$$

Solving for i_{osc}

$$i_{\mathrm{osc}}(s) = Y(s)u_{\mathrm{osc}}(s) \tag{33}$$

where $Y(s)$ can be expressed as

$$Y(s) = G_v(s)G_i(s)[Z_o(s)I + Z^0(s)A]^{-1}. \tag{34}$$

To compartmentalize the nonlinear and linear part of the system, the matrix form of (17) can be expressed as

$$u_{\mathrm{osc}}(s) = M_{\mathrm{osc}}(i_f(s) - i_{\mathrm{osc}}(s)) \tag{35}$$

where $i_f(s) \triangleq [i_{f1}(s), i_{f2}(s), \ldots, i_{fn}(s)]^T$, $M_{\mathrm{osc}}(s) \triangleq Z_{\mathrm{osc}}(s)I$.

Substituting (33) into (35) and solving for $v_{\mathrm{osc}}(s)$ yields

$$u_{\mathrm{osc}}(s) = [I - M_{\mathrm{osc}}(s)Y(s)]^{-1}M_{\mathrm{osc}}(s)i_f(s). \tag{36}$$

Define the vector of nonlinear function

$$f(u_{\mathrm{osc}}(s)) \triangleq [f(u_{\mathrm{osc}1}(s)), f(u_{\mathrm{osc}2}(s)), \ldots, f(u_{\mathrm{osc}n}(s))]^T. \tag{37}$$

Thus, the nonlinear part of the system can be expressed as

$$i_f(s) = f(u_{\mathrm{osc}}(s)). \tag{38}$$

The model of the system with nonlinear and linear part divided can be depicted in Fig. 9. The theorem establishing a sufficient condition for the global asymptotic synchronization of virtual oscillator can be expressed as the following:

$$\sup_{\omega\in\mathbb{R}} \left\| \frac{(G_u(j\omega)G_i(j\omega))^{-1}Z_o(j\omega)Z_{\mathrm{osc}}(j\omega)}{(G_u(j\omega)G_i(j\omega))^{-1}Z_o(j\omega) + Z_{\mathrm{osc}}(j\omega)} \right\| \sigma < 1. \tag{39}$$

The proof of (39) have been given in [20][3] and will not be duplicated here

[3]If ν and ι is replaced with $G_u(s)$ and $G_i(s)$ respectively, the condition proofed in [20] is exactly same as in this paper.

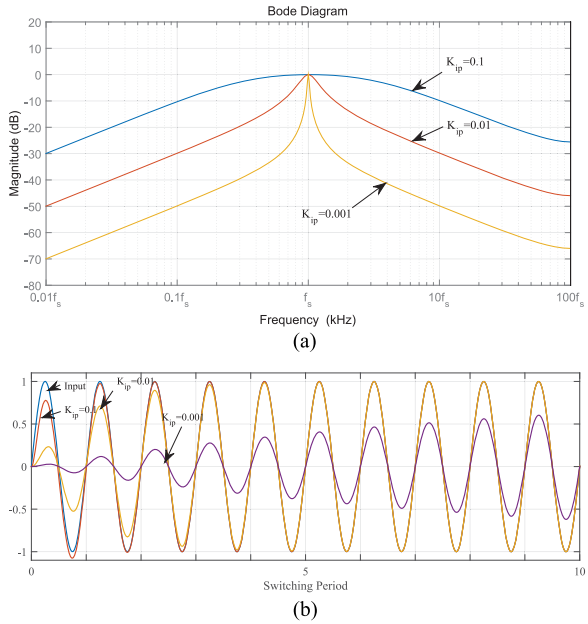

Fig. 10. (a) Bode diagram of $G_f(z)$ with different $K_{\rm ip}$. (b) Dynamic response of filter with different $K_{\rm ip}$.

IV. Parameter Selection

In this section, the process for the controller parameter selection is outlined including the bandpass filter and virtual oscillator.

A. Bandpass Filter

The purpose of bandpass filter is to filter out components other than that of switching frequency. Hence, the design is based on two principals: 1) The attenuation and phase shift on switching frequencies should be as small as possible. 2) The attenuation on the harmonics of the switching frequency and base frequency should be large enough to eliminate their effects on the virtual oscillator. 3) The delay of the filter should not degrade the dynamic performance of the system.

One possible example of such digital bandpass filter can be expressed as

$$G_{fo} = \frac{K_{\rm ip}(z-1)}{z^2 - 2z\cos(2\pi f_{\rm sw}/f_s) + 1}$$
$$G_f = \frac{G_{fo}(z)}{1 + G_{fo}(z)} \tag{40}$$

where $K_{\rm ip}$ is the integral constant of the filter, $f_{\rm sw}$ the switching frequency, f_s is the sampling frequency. The open-loop transfer function $G_{fo}(z)$ imposes high magnitude and zero phase shift on the switching frequency so that the close-loop transfer function $G_f(z)$ can be regarded as the bandpass filter conforming to the principals.

The magnitude and phase response of $G_f(z)$ with different $K_{\rm ip}$ is shown in Fig. 10(a). It can be concluded that the smaller $K_{\rm ip}$ results the better attenuation ability of the filter. Therefore the $K_{\rm ip}$ should be designed small enough to achieve high attenuation of base frequency current for its amplitude can be much larger than the switching frequency one.

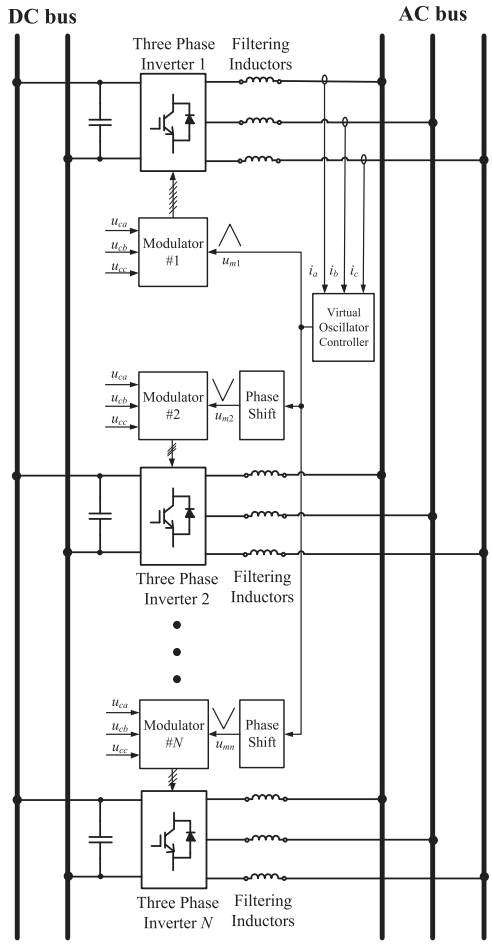

Fig. 11. Simulation used to perform test to select the current gain k_i.

TABLE I
Experimental Parameters

Prototype Parameters			Controller Parameters		
Rated frequency	f	50 Hz	Virtual Oscillator Inductance	L_E	2.533 μH
Filter Inductance	L	3 mH	Virtual Oscillator Capacitor	C_E	20 mF
Filter Capacitor	C	20 μF	Virtual Oscillator Resistor	R_E	10 Ω
Switching Frequency	$f_{\rm sw}$	1000 Hz	Slope of nonlinear current source	σ	1 S
Load per phase	R_L	3.7 Ω	Turning point of nonlinear current source	φ	0.55 V
DC bus voltage	$U_{\rm dc}$	30 V	Current Gain	k_i	0.5
			Integral constant of the filter	$K_{\rm ip}$	0.01
			Sampling Frequency	f_s	200 kHz

Another consideration of the designation of $K_{\rm ip}$ is its effects on the dynamic performance of system. As shown in Fig. 10(b), the lower $K_{\rm ip}$ will make filter to spend more time to reach its desired output and degrade the dynamic performance of the whole system. Thus, the $K_{\rm ip}$ should be chosen to ensure the delay of the filter should not exceed half of the period of base frequency of the system.

B. Virtual Oscillator

The design selection can be formulated as follows: Given the filter independence Z_o and rated switching frequency $\omega_{\rm sw}$,

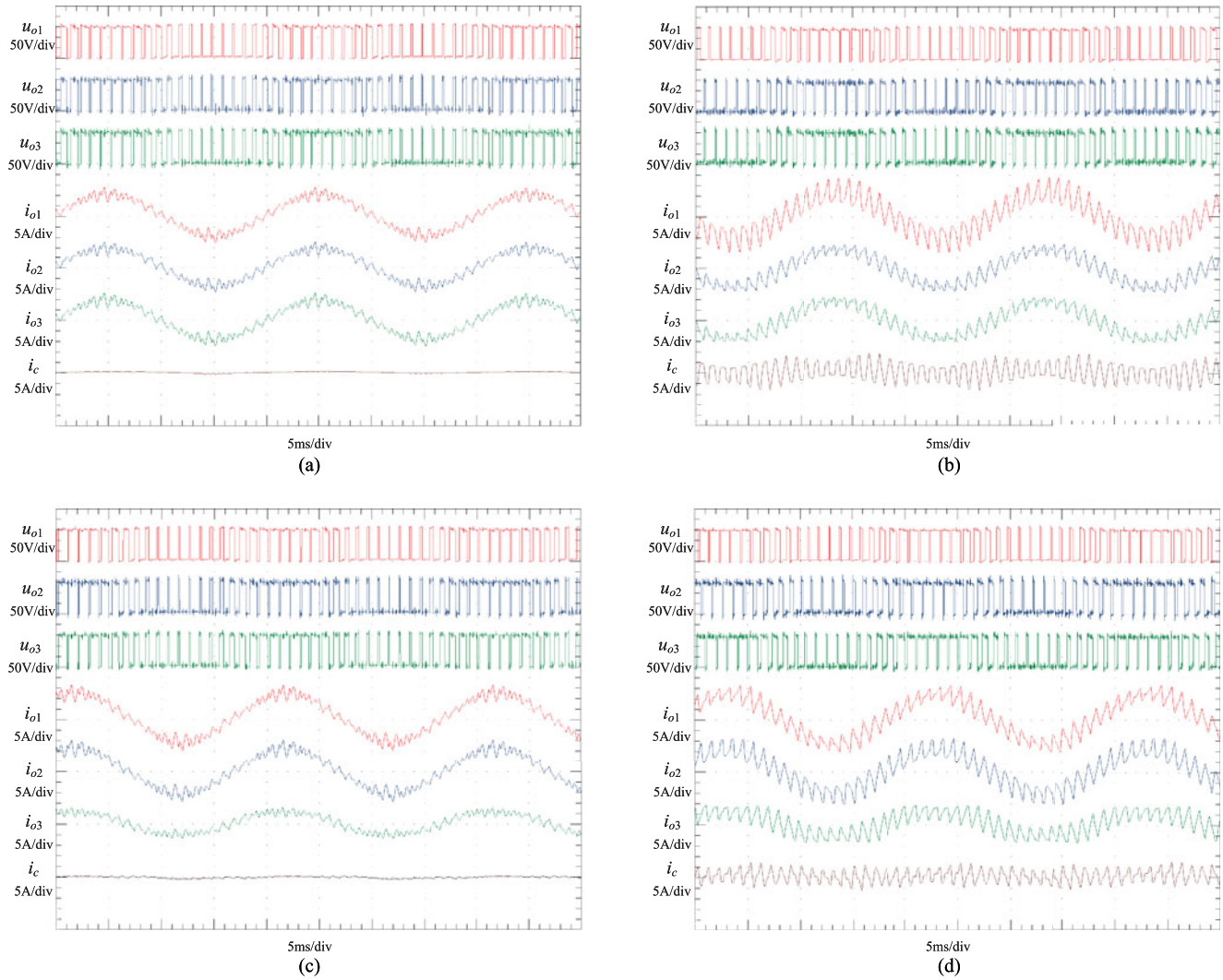

Fig. 12. Steady-state experimental results. Waveforms in (a) and (b) demonstrate the steady state of system with and without carrier wave synchronization when under 1 : 1 : 1 ratios of power sharing. Waveforms in (c) and (d) demonstrate the steady state of system with and without carrier wave synchronization when under 2 : 2 : 1 ratios of power sharing.

select the current gain k_i and virtual oscillator parameters R_E, L_E, C_E, φ, and σ to ensure that 1) the condition of the global asymptotic synchronization is satisfied and 2) the switching frequency is maintained within the prescribed upper and lower limits under worst case.

The selection of parameter is performed according to selected as following steps:

1) The inductance and capacitor L_E and C_E is selected to ensure the frequency of oscillator $f_{\rm osc}$ to be the desired switching frequency $f_{\rm sw}$ based on (15).
2) Let $\sigma = 1$ and select $R_E > 1/\sigma$.
3) Set $i_{\rm osc} = 0$, run simulation in Fig. 5, turn φ to make sure the amplitude of oscillator $A_{\rm osc}$ reach the desired value.
4) The worst working condition of the controller is that all the other inverters have the opposite carrier waves. In order to investigate the behavior of the virtual oscillator under such condition, simulation is performed in the system depicted in Fig. 11. The phase current of one inverter is used to generate the modulation wave with the VOC depicted in Fig. 7(a), the generated modulation wave u_{m1} is used to generate the drive signal of the inverter. While, the modulation waves of the other inverters are generated by phase shift block which shift the u_{m1} by 180°. Thus, the other inverters always have the opposite carrier waves. Using this model, the current gain k_i is tuned to keep the switching frequency within the desired range even under worst cases.
5) The condition (39) is checked in order to ensure the global asymptotic synchronization of the system. If the condition is not satisfied, decrease σ and return to step 2.
6) The sampling frequency f_s is selected to be much larger than the switching frequency $f_{\rm sw}$ to ensure the accuracy of the synchronization.

V. Experimental Results

In order to test the effectiveness and stability of the proposed control, a 20 times scaled-down experimental prototype

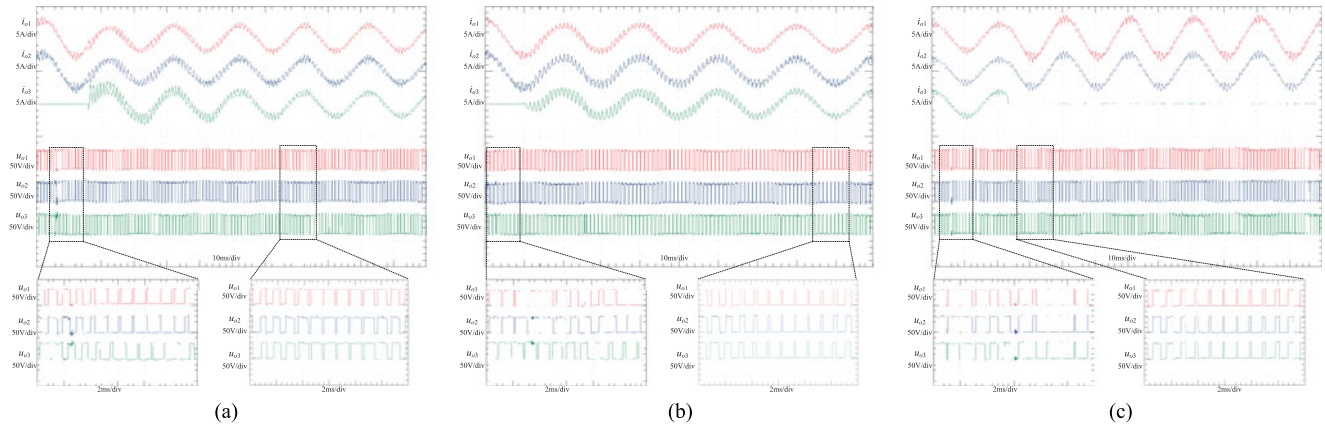

Fig. 13. Experiment results of transient behavior. Waveforms in (a) and (b) demonstrate the transient behavior of system with inverter addition under 0.01 and 0.001 k_{ip}. Waveforms in (c) correspond to the case of inverter removal.

consisting of three three-phase inverters connected parallel is built and tested in this section. As the parallel operation of inverter often operates at high current circumstances, the load impedance is set low as 3.7 Ω. Under high power rating circumstances, the switching frequency could not be high for the limitation of the power loss, the switching frequency is set as 1 kHz. Due to the low switching frequency, the filter parameters are set large to achieve enough attenuation of switching ripples. The detailed electrical schematic of the system is the same as in Fig. 3. The controller is implemented by using a Texas Instruments TMS320F28335 digital signal processor. The virtual oscillator is digitalized as follows: (16) is realized by if-else structure and (17) is achieved by a two-order discrete transfer function. The detailed parameters of the prototype and controller can be found in Table I.

A. Steady State

First, the ratios of power sharing of three inverters are set as 1 : 1 : 1. Then, a comparison between the steady state of the parallel inverter system sharing with and without carrier wave synchronization is carried out to justify the effectiveness of the proposed control. Each inverter's output voltage and current of phase A bridge is shown in Fig. 12(a) and (b). The circulating current i_c of inverter 1 is calculated by: $i_c = i_{o1} - i_l/3$ [21].

As shown in Fig. 12(b), without carrier wave synchronization, the circulating current consists of the switching frequency component and its the amplitude is over 2 A and is mainly consist of switching frequency components. If the carrier waves are synchronized as depicted in Fig. 12(a), the switching frequency components are completely eliminated.

Next, the ratios of power sharing of three inverters are changed to 2:2:1. Similar comparison is made and in this case, the circulating current is calculated by $i_c = i_{o1} - 2i_l/5$ [22].

Similar to the case with same power sharing, as shown in Fig. 12(d), without carrier wave synchronization, the circulating current is mainly consist of switching frequency components with amplitude of over 2 A. If the carrier waves are synchronized as depicted in Fig. 12(c), the switching frequency components are eliminated.

Therefore, it can be concluded that the synchronization of the carrier wave greatly reduced the switching frequency circulating current among different inverters both under identical or nonidentical cases.

B. Inverter Addition and Removal

Next, the dynamic behavior of the proposed control with inverter addition is performed. Fig. 13(a) shows the transient response of the system as a third inverter is added to the system with K_{ip} of 0.01. 50 ms after the addition, the synchronization is achieved and the circulating current disappears. When K_{ip} is set as 0.001, as Fig. 13(b) shows, the system cost more time to synchronize the carrier wave. Even after 80 ms after the transient, the carrier waves of three inverters have not been fully synchronized. Thus, the K_{ip} should be set correctly to achieve good performance of the system.

Transient behavior of the inverter removal is shown in Fig. 13(c). It can be concluded that the removal of the inverter does not affect the synchronization of carrier wave of the remaining inverters since the carrier waves of them remain synchronized after the removal. Thus, the stability of the system remains after inverter removal.

VI. Conclusion and Future Work

A method for synchronizing carrier wave of different inverters in a parallel three-phase inverter system is presented in this paper. The proposed technique relies on the virtual oscillators of inverters that emulate the coupling oscillator networks to synchronize with each other. It is shown that inverters of the parallel inverter system can synchronize their carrier wave without communication. This will greatly reduce the complexity of the control system if synchronization of carrier waves of a parallel inverter system is needed. A sufficient condition for virtual oscillator synchronization is derived and the results suggest that this method is independent of the load and the number of inverters. In addition, a methodology to determined the parameters of the controller are also given. Finally, experiments are conducted

and the corresponding results justify the effectiveness of the proposed strategy.

Compelling avenues for future work include developing similar controllers for grid-connected applications. Furthermore, this method should be extended to other modulation method such as space-vector PWM or discontinuous PWM. Finally, future efforts could be focused on the analytically quantifying the dynamic performance of the proposed control.

REFERENCES

[1] Y. Zhang and H. Ma, "Theoretical and experimental investigation of networked control for parallel operation of inverters," *IEEE Trans. Ind. Electron.*, vol. 59, no. 4, pp. 1961–1970, Apr. 2012.

[2] T.-F. Wu, H.-M. Hsieh, Y.-E. Wu, and Y.-K. Chen, "Parallel-inverter system with failure isolation and hot-swap features," *IEEE Trans. Ind. Appl.*, vol. 43, no. 5, pp. 1329–1340, Sep./Oct. 2007.

[3] J. F. Chen and C. L. Chu, "Combination voltage-controlled and current-controlled PWM inverters for UPS parallel operation," *IEEE Trans. Power Electron.*, vol. 10, no. 5, pp. 547–558, Sep. 1995.

[4] M. Borrega, L. Marroyo, R. Gonzalez, J. Balda, and J. L. Agorreta, "Modeling and control of a master-slave PV inverter with n-paralleled inverters and three-phase three-limb inductors," *IEEE Trans. Power Electron.*, vol. 28, no. 6, pp. 2842–2855, Jun. 2013.

[5] R. I. Bojoi, L. R. Limongi, D. Roiu, and A. Tenconi, "Enhanced power quality control strategy for single-phase inverters in distributed generation systems," *IEEE Trans. Power Electron.*, vol. 26, no. 3, pp. 798–806, Mar. 2011.

[6] C.-T. Pan and Y.-H. Liao, "Modeling and coordinate control of circulating currents in parallel three-phase boost rectifiers," *IEEE Trans. Ind. Electron.*, vol. 54, no. 2, pp. 825–838, Apr. 2007.

[7] Z. H. Ye, D. Boroyevich, J. Y. Choi, and F. C. Lee, "Control of circulating current in two parallel three-phase boost rectifiers," *IEEE Trans. Power Electron.*, vol. 17, no. 5, pp. 609–615, Sep. 2002.

[8] X. Zhang, J. Chen, Y. Ma, Y. Wang, and D. Xu, "Bandwidth expansion method for circulating current control in parallel three-phase PWM converter connection system," *IEEE Trans. Power Electron.*, vol. 29, no. 12, pp. 6847–6856, Dec. 2014.

[9] T. Itkonen, J. Luukko, A. Sankala, T. Laakkonen, and R. Pollanen, "Modeling and analysis of the dead-time effects in parallel PWM two-level three-phase voltage-source inverters," *IEEE Trans. Power Electron.*, vol. 24, no. 11, pp. 2446–2455, Nov. 2009.

[10] T. B. Lazzarin, G. A. T. Bauer, and I. Barbi, "A control strategy for parallel operation of single-phase voltage source inverters: Analysis, design and experimental results," *IEEE Trans. Ind. Electron.*, vol. 60, no. 6, pp. 2194–2204, Jun. 2013.

[11] T. F. Wu, Y. K. Chen, and Y. H. Huang, "3C strategy for inverters in parallel operation achieving an equal current distribution," *IEEE Trans. Ind. Electron.*, vol. 47, no. 2, pp. 273–281, Apr. 2000.

[12] T.-P. Chen, "Zero-sequence circulating current reduction method for parallel HEPWM inverters between AC bus and DC bus," *IEEE Trans. Ind. Electron.*, vol. 59, no. 1, pp. 290–300, Jan. 2012.

[13] H. Ma, Z. Lin, L. Dong, and Q. Guo, "Modeling and analysis of switching frequency circulating current in three-phase parallel inverters," in *Proc. IEEE Ind. Electron. Conf.*, 2014, pp. 568–573.

[14] D. Shin, K.-J. Lee, H.-J. Kim, J.-P. Lee, T.-J. Kim, and D.-W. Yoo, "Coupled inductors for parallel operation of interleaved three-phase voltage source grid-connected inverters," in *Proc. IEEE Appl. Power Electron. Conf.*, 2013, pp. 2235–2239.

[15] H. Cai, R. Zhao, and H. Yang, "Study on ideal operation status of parallel inverters," *IEEE Trans. Power Electron.*, vol. 23, no. 6, pp. 2964–2969, Nov. 2008.

[16] C. Song, R. Zhao, M. Zhu, and Z. Zeng, "Operation method for parallel inverter system with common DC link," *IET Power Electron.*, vol. 7, no. 5, pp. 1138–1147, 2014.

[17] M. Yiwei, Y. Liu, W. Jing, S. Xiaojie, F. Wang, and L. M. Tolbert, "Circulating current control and reduction in a paralleled converter testbed system," in *Proc. IEEE Energy Convers. Congr. Expo. Conf.*, 2013, pp. 5426–5432.

[18] S. V. Dhople, B. B. Johnson, F. Doerfler, and A. O. Hamadeh, "Synchronization of nonlinear circuits in dynamic electrical networks with general topologies," *IEEE Trans. Circuits Syst. I, Reg. Papers*, vol. 61, no. 9, pp. 2677–2690, Sep. 2014.

[19] B. B. Johnson, S. V. Dhople, J. L. Cale, A. O. Hamadeh, and P. T. Krein, "Oscillator-based inverter control for islanded three-phase microgrids," *IEEE J. Photovoltaics*, vol. 4, no. 1, pp. 387–395, Jan. 2014.

[20] B. B. Johnson, S. V. Dhople, A. O. Hamadeh, and P. T. Krein, "Synchronization of parallel single-phase inverters with virtual oscillator control," *IEEE Trans. Power Electron.*, vol. 29, no. 11, pp. 6124–6138, Nov. 2014.

[21] C.-T. Pan and Y.-H. Liao, "Modeling and coordinate control of circulating currents in parallel three-phase boost rectifiers," *IEEE Trans. Ind. Electron.*, vol. 54, no. 2, pp. 825–838, Apr. 2007.

[22] C.-T. Pan and Y.-H. Liao, "Modeling and control of circulating currents for parallel three-phase boost rectifiers with different load sharing," *IEEE Trans. Ind. Electron.*, vol. 55, no. 7, pp. 2776–2785, Jul. 2008.

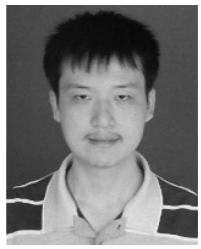

Jian Hu (S'15) was born in Nanjing, China, in 1990. He received the B.S.E.E. degree from Southeast University, Nanjing, China. He is currently working toward the Ph.D. degree in the College of Electrical Engineering, Zhejiang University, Hangzhou, China.

His research interests include power electronics equipment, renewable energy, power quality, and parallel operation of the inverter.

Hao Ma (M'99) was born in Hangzhou, China, in 1969. He received the B.Sc., M.Sc., and Ph.D. degrees in electrical engineering from Zhejiang University, Hangzhou, China, in 1991, 1994, and 1997, respectively.

He is currently a Professor with the College of Electrical Engineering, Zhejiang University. From September 2007 to September 2008, he acted as a Delta Visiting Scholar at North Carolina State University, Raleigh, NC, USA. His research interests include advanced control in power electronics, fault diagnosis of power electronic circuits and systems, and application of power electronics.